frontiers in Nanotechnology

ORIGINAL RESEARCH
published: 27 April 2021
doi: 10.3389/fnano.2021.653744

Detection and Aggregation of *Listeria Monocytogenes* Using Polyclonal Antibody Gold-Coated Magnetic Nanoshells Surface-Enhanced Raman Spectroscopy Substrates

Robert T. Busch[1], *Farzia Karim*[2], *Yvonne Sun*[3,4], *H. Christopher Fry*[5], *Yuzi Liu*[5], *Chenglong Zhao*[2,6] *and Erick S. Vasquez*[1,4]*

[1]Department of Chemical and Materials Engineering, University of Dayton, Dayton, OH, United States, [2]Department of Electro-Optics and Photonics, University of Dayton, Dayton, OH, United States, [3]Department of Biology, University of Dayton, Dayton, OH, United States, [4]Integrative Science and Engineering Center, University of Dayton, Dayton, OH, United States, [5]Center for Nanoscale Materials, Argonne National Laboratory, Lemont, IL, United States, [6]Department of Physics, University of Dayton, Dayton, OH, United States

OPEN ACCESS

Edited by:
Amit Kumar Mandal,
Raiganj University, India

Reviewed by:
Satyabrata Mohapatra,
Guru Gobind Singh Indraprastha University, India
Nilay Ildız,
Erciyes University, Turkey
Ahmet Katı,
University of Health Sciences, Turkey
Mehmet Kahraman,
University of Gaziantep, Turkey

***Correspondence:**
Erick S. Vasquez
evasquez1@udayton.edu

Specialty section:
This article was submitted to Biomedical Nanotechnology, a section of the journal Frontiers in Nanotechnology

Received: *15 January 2021*
Accepted: *12 April 2021*
Published: *27 April 2021*

Citation:
Busch RT, Karim F, Sun Y, Fry HC, Liu Y, Zhao C and Vasquez ES (2021) Detection and Aggregation of Listeria Monocytogenes *Using Polyclonal Antibody Gold-Coated Magnetic Nanoshells Surface-Enhanced Raman Spectroscopy Substrates. Front. Nanotechnol. 3:653744. doi: 10.3389/fnano.2021.653744*

Magnetic nanoshells with tailored surface chemistry can enhance bacterial detection and separation technologies. This work demonstrated a simple technique to detect, capture, and aggregate bacteria with the aid of end-functionalized polyclonal antibody gold-coated magnetic nanoshells (pAb-Lis-AuMNs) as surface-enhanced Raman spectroscopy (SERS) probes. *Listeria monocytogenes* were used as the pathogenic bacteria and the pAb-Lis-AuMNs, 300 nm diameter, were used as probes allowing facile magnetic separation and aggregation. An optimized covalent bioconjugation procedure between the magnetic nanoshells and the polyclonal antibody was performed at pH six *via* a carbodiimide crosslinking reaction. Spectroscopic and morphological characterization techniques confirmed the fabrication of stable pAb-Lis-AuMNs. The resulting pAb-Lis-AuMNs acted as a SERS probe for *L. monocytogenes* based on the targeted capture *via* surface binding interactions and magnetically induced aggregation. Label-free SERS measurements were recorded for the minimum detectable amount of *L. monocytogenes* based on the SERS intensity at the 1388 cm^{-1} Raman shift. *L. monocytogenes* concentrations exhibited detection limits in the range of 10^4–10^7 CFU ml^{-1}, before and after aggregation. By fitting these concentrations, the limit of detection of this method was ~10^3 CFU ml^{-1}. Using a low-intensity magnetic field of 35 G, pAb-Lis-AuMNs aggregated *L. monocytogenes* as demonstrated with microscopy techniques, including SEM and optical microscopy. Overall, this work presents a label-free SERS probe method comprised of a surface-modified polyclonal antibody sub-micron magnetic

Abbreviations: pAb, polyclonal antibody; AuMNs, gold coated iron oxide nanoparticles; pAb-Lis-AuMNs, polyclonal antibody gold-coated magnetic nanoshells; MES, 2-(N-morpholino) ethanesulfonic acid; EDC, N-(3-(dimethylaminopropyl) -N′-carbodiimide; NHS, N-Hydroxysuccinimide; PBS, phosphate buffer solution; DLS, dynamic light scattering; UV-Vis, ultraviolet-visible spectroscopy; FT-IR, fourier transform infrared spectroscopy; TEM, transmission electron microscopy; HR-SEM, high-resolution scanning electron microscopy; SERS, surface enhanced raman spectroscopy; PCR, polymerase chain reaction; EF, enhancement factor; LOD, limit of detection; ANOVA, analysis of variance; TOST, two-one-sided t-test; CFU, colony forming units.

nanoshell structures with high sensitivity and magnetic induced separation that could lead to the fabrication of multiple single-step sensors.

Keywords: *listeria monocytogenes*, polyclonal antibody, gold-coated magnetic nanoshells, SERS detection, magnetic separation, surface functionalization, bioconjugation chemistry

INTRODUCTION

L. monocytogenes is a well-known foodborne pathogen with a ubiquitous presence in the environment, complicating its elimination from food production processes (Thakur et al., 1991; Law et al., 2015; Buchanan et al., 2017; Liu et al., 2017). Consumption of *L. monocytogenes*-contaminated foods can cause listeriosis, exhibiting a high fatality rate ranging between 20 and 30% in high-risk individuals (Hoffmann et al., 2012). As a result, food products with *L. monocytogenes* count levels higher than 100 colony-forming units (CFU)/g have been unacceptable for human consumption in Europe (Food and Authority, 2013). In the United States, any detection of *L. monocytogenes* CFU per 25 g of ready-to-eat food products is unacceptable, a practice referred to as the zero-tolerance policy (U.S. FDA, 2020). Current high specificity detection methods with sensing limits acceptable for this range can take longer than 1 day for results (Mandal et al., 2011). As such, the development and optimization of rapid and sensitive detection methods for *L. monocytogenes* can be extremely beneficial to prevent foodborne outbreaks.

The use of magnetite and gold nanoparticles has increased recently to detect and eliminate pathogens with a rapid and sensitive methodology (Fratila et al., 2014; Liu et al., 2017; Sposito et al., 2018). Silver and gold-coated iron oxide nanospheres have recently garnered attention as competitive sub-micron sized, multifunctional particles (Wang et al., 2008; 2016a). These sub-micron particles maintain desirable superparamagnetic properties due to the presence of iron oxide in its core in addition to pristine surface properties, enhanced electrostatic repulsion, and protection from oxidation from the rough-surface gold coating (Bao et al., 2009; Yueming et al., 2009). These properties allow for force-controlled spatial manipulation of bacteria, including *L. monocytogenes*, and provide a tag to enhance scattering for detection methods such as Raman spectroscopy (Dörig et al., 2010). However, to improve adsorption capabilities, specific binding interactions between particles and *L. monocytogenes* are necessary (Zhang et al., 2015).

Several molecules demonstrate the potential for the surface modification of gold-coated nanoparticles to detect pathogens such as bacteria. These types of molecules include peptides, oligonucleotides, enzymes, and antibodies (Fratila et al., 2014; Zhang et al., 2017). Antibodies are desirable due to their availability, quality, and specificity toward a particular specimen (Lipman et al., 2013). Additionally, the vast array of charged moieties throughout the protein structure allows for chemisorption to particles through covalent bonding or electrostatic stabilization *via* ionic or hydrophobic interactions (Montenegro et al., 2013; Busch et al., 2019). By employing carboxyl surface-functionalized (—COOH), gold-magnetic structures, antibodies can be covalently bound to their surfaces, producing stable pathogen detecting particles (Welch et al., 2017). This procedure has frequently been established through a common carbodiimide crosslinker chemistry using 1-(3-dimethylaminopropyl)-3-ethylcarbodiimide hydrochloride-N-hydroxysuccinimide (EDC-NHS) (Bartczak and Kanaras, 2011; Zhang et al., 2017). This specific antibody-particle bioconjugate formation allows an analysis of pathogen capture and detection enhancements.

A promising technique for precise and sensitive detection of biological entities is surface-enhanced Raman spectroscopy (SERS) due to the ability to receive "fingerprint" of chemical and biochemical molecules (Grubisha et al., 2003; Granger et al., 2016). Recently, the development of new SERS-based sensors has explored the use of various substrates, including gold, silver, and other metal nanoparticles (Granger et al., 2016; Shibusawa et al., 2019; Chen et al., 2020). This development has spurred the design of advanced multifunctional biosensors, including the use of magnetization—a property found in nanocomposites comprised of magnetic nanoparticles and another metal such as gold—to further increase pathogen detection and removal (**Figure 1**). Within this category, there are two primary techniques for detection—label-based methods and label-free methods. Label-based approaches utilize a signal probe that becomes the primary detectable material. For example, tuned gold nanorods (AuNRs) develop a particularly strong peak resonating with the localized surface plasmon resonance (LSPR) of the AuNRs; thus, allowing the AuNRs to act as an enhanced primary reporter (Nikoobakht and El-Sayed, 2003; Sharma et al., 2016). By comparison, label-free methods maintain the bacteria's detection without any label to maintain the SERS spectrum intrinsic to the pathogens of interest (Jarvis and Goodacre, 2008; Wu et al., 2015; Wang et al., 2019).

This study describes the functionalization of gold-coated iron oxide nanoshells (AuMNs) with a polyclonal *L. monocytogenes* antibody (pAb-Lis) for use as a SERS-based biosensor through a covalent coupling surface functionalization step. Polyclonal antibody modified AuMNs (pAb-Lis-AuMNs) were grafted onto the AuMNs following a unique, optimized bioconjugation protocol at pH six to cover the AuMNs completely with properly aligned pAb-Lis (Busch et al., 2019). We confirm the formation of the pAb-Lis-AuMN complexes through chemical and morphological characterization. These functionalized nanoshells were utilized as a single step Raman probe to maintain direct detection and aggregation of *L. monocytogenes* using SERS and a rare Earth permanent magnet. The pAb-Lis-AuMNs adhered to *L. monocytogenes* walls, aggregating the pathogen before collecting Raman spectra using an external magnet. Raman spectroscopy signal intensities were recorded to determine the limit of detection (LOD) for *L. monocytogenes*. To our knowledge, this is one of

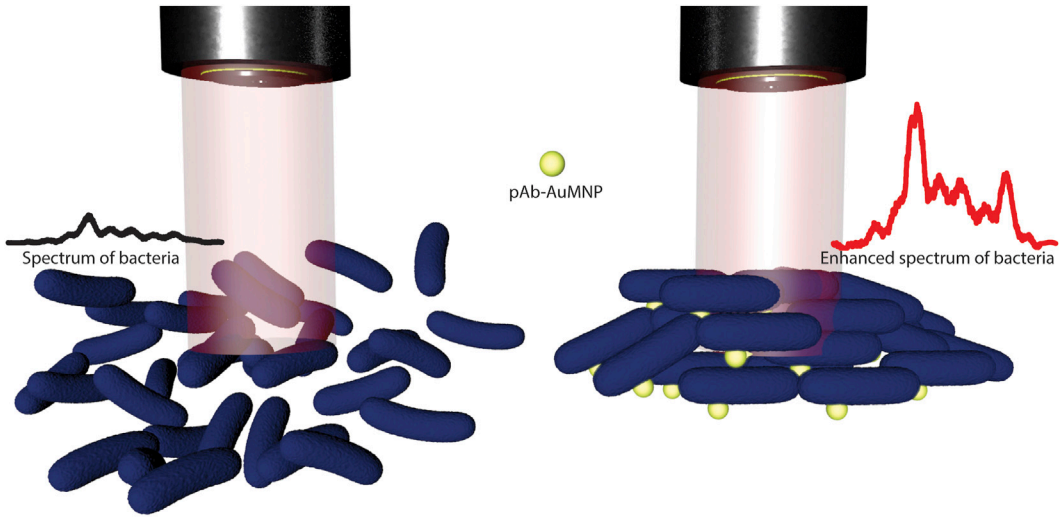

FIGURE 1 | Schematic illustration of label-free SERS method for bacteria detection using functionalized Au magnetic nanoshells (pAb-Lis-AuMNs). The scheme depicts a multilayer bacteria/pAb-Lis-AuMNs structure which induce an enhanced spectrum of the bacteria and a facile magnetic separation under the presence of a 35 Gauss magnetic field.

the first studies that use a polyclonal antibody against *L. monocytogenes* covalently bonded onto the surface of a gold-coated multicore magnetic cluster (~280 nm). We found the LOD to be between 10^4 and 10^5 CFU ml^{-1} before addition of the pAb-Lis-AuMNs and an LOD of ~10^3 CFU ml^{-1} after addition and aggregation of pAb-Lis-AuMNs under the presence of a 35 Gauss magnetic field. Additionally, we report a nearly 7 times peak Raman intensity enhancement following magnetic aggregation of the particles at a constant AuMN to *L. monocytogenes* ratio and an enhancement factor (EF) of $10^{4.4}$. In addition, we confirm the binding and aggregation of the pAb-Lis-AuMNs to the *L. monocytogenes* through SEM and Gram-stained optical microscopy images.

MATERIALS AND METHODS

Materials

N-(3-(dimethylaminopropyl) -N′-carbodiimide (EDC, 97%), N-Hydroxysuccinimide (NHS, 98%), 2-(N-Morpholino) ethanesulfonic acid (MES, 99.5%), 2-(N-Morpholino) ethanesulfonic acid sodium salt (NaMES, 99%), Hydroxylamine 50 weight% in water, and isopropyl alcohol (IPA, 98%) were purchased from Sigma-Aldrich (St. Louis, MO, United States). 280 nm Magnetic Gold Nanoshells (Bio-Ready, carboxyl, 20 OD, 1 ml, water) were obtained from NanoComposix (San Diego, CA, United States) and used for SERS probes based on previous work (Karim et al., 2019). 16% paraformaldehyde was purchased from Alfa Aesar (Ward Hill, MA, United States). A rabbit polyclonal antibody against *Listeria monocytogenes,* pAb-Lis (PA130487), was obtained from Fisher Scientific™ and used as-received without further purification. All the reagents were used as received. Ultrapure type-1 water (18 MΩ-cm) was acquired from an Elga PURELAB purification system and was used for buffer and solution preparations.

Surface Functionalization of Gold-Coated Magnetic Nanoshells (AuMNs) Using pAb-Lis

EDC and NHS solutions were prepared at concentrations of 2 and 10 mg/ml, respectively, using DI water. 200 µl of the 280 nm carboxylated magnetic gold nanoshells (AuMNs) aqueous suspension was transferred to CCPO micro-centrifuge tubes from Fisher Scientific, which were pre-washed with isopropyl alcohol and DI water. For the bioconjugation procedure of the pAb onto the AuMNs, an previously reported protocol is utilized, with slight modifications for larger gold coated particles (Busch et al., 2019). Briefly, 1 ml of pH six MES buffer solution was added to the 200 µl AuMNs suspension to begin pH control. 20 µl of 2 mg/ml EDC solution was added to the 1.2 ml of AuMNs colloidal suspension. This suspension was vortexed at 1000 RPM at room temperature for 10 min 8 µl of 10 mg/ml NHS solution was added to the EDC/AuMNs suspension. This suspension was vortexed at 1000 RPM at room temperature for 10 min. The suspension was then centrifuged at 15,000 RCF for 10 min at 10°C. The supernatant was carefully removed, and the remaining AuMNs pellet was re-suspended with 200 µl of 25 mM MES buffer prepared at pH six. Resuspension was performed by sonicating the solution for 5 min and vortex-mixing for 5 min at 1000 RPM. This washing procedure was repeated twice followed by off-line DLS measurements using 20 µl of the suspension in 1.5 ml of DI water. Then, 8 µl of 1 mg/ml antibody solution was added to the AuMNs colloidal suspension for 60 min. The AuMN pellet was resuspended in 200 µl of DI water, and 1 µl of quencher (50% hydroxylamine) was added to the suspension. Subsequently, the

colloidal suspension was split into two 100 µl aliquots, placed in CCPO micro-centrifuge tubes and centrifuged at 15,000 RCF for 10 min at 10°C, and resuspended in DI water. This washing procedure was repeated three times.

Binding Evaluation of pAb-Lis Onto AuMNs (pAb-Lis-AuMNs)

Transmission Electron Microscopy (TEM) images were collected with a JEOL 2100 TEM instrument at 200 kV. AuMNs colloid (5 µl) was added to copper carbon mesh grid (CF300-Cu; EMS Sciences). The tweezers (Fontax #16), holding the grid, were then placed under vacuum for 15 min. The sample was then removed from the chamber and allowed to dry for an additional 30 min at room temperature before imaging in the TEM.

Fourier Transform Infrared Spectroscopy (FT-IR) data were collected using a Nicolet iS50 FT-IR spectrometer equipped with an attenuated total reflection (ATR) attachment (Smart Golden Gate, ZnSe lens, Thermo Electron North America LLC). A minimum of 128 scans was collected, with the background spectrum collected after each sample. Liquid nitrogen cooled (MCT-A) detector with CdTe window ZnSe crystal was utilized, and data was collected using OMNIC Software Suite v 7.3. AuMNs and pAb-Lis-AuMNs aliquots of 10 µl were placed directly onto the ATR crystal and allowed to dry for approximately 40 min until a thin film remained. The reference spectrum for each sample was taken under identical conditions after the ATR crystal was cleaned with isopropyl alcohol.

Dynamic Light Scattering (DLS) was used to obtain effective diameters of the AuMNs at different bioconjugation steps. A NanoBrook 90 Plus with a red laser (640 nm) and a 90° scattering angle was used. For all measurements, a 1 cm × 1 cm quartz cuvette was used. For each sample, five DLS measurements were conducted with ten repetitions, and average results are reported. The off-line DLS samples were prepared as a 1:20 dilution by volume from the prepared solution with DI water.

Average ζ-potential values were recorded using a Malvern Zetasizer instrument with a minimum of 200 and a maximum of 600 runs until a standard deviation of less than 0.1 mV was achieved at 25°C. Samples of AuMNs, pAb-Lis-AuMNs, and neat pAb-Lis at 200 µl:1 ml dilution using 1X, 7.4 pH PBS were mixed before being placed in a folded capillary z cell (Malvern Panalytical).

L. Monocytones: Bacterial Strain and Culture Conditions

Cultures of the wild type *L. monocytogenes* strain 10403 s were grown from colonies on a freshly streaked brain-heart infusion (BHI) plate at 37°C. Bacteria were grown overnight in BHI media within a 37°C incubator while at 250 RPM for adequate oxygen diffusion. Optical density (OD) was measured in a 96-well plate at 600 nm with a volume of 200 µl per well using a 96-well plate reader (Synergy 4, Biotek, Winooski, VT, United States). The OD values are used to calculate the bacterial counts in CFU per ml by using the following formula: An OD value of one is equivalent to 6.6×10^8 CFU per ml.

Detection and Aggregation of *L. monocytogenes* Using *S*urface-Enhanced Raman Scattering (SERS) Polyclonal Antibody Gold-coated Magnetic Nanoshells

All SERS data were recorded with a Raman spectrometer (Renishaw in *via* Reflex Micro-Raman) equipped with a near-infrared diode laser source (maximum laser power: 300 mW, laser wavelength: 785 nm). To get maximum Raman signal from the sample, Raman exciting laser was focused on the samples with a microscope objective lens (50×, NA = 0.75). Laser power on the sample was kept at 30 mW (10% of maximum laser power, 300 mW). Raman signals from all samples were collected for 10 s exposure time using 10 µl samples on glass slides, covering a diameter of approximately 1 cm. For this method the pAb-Lis-AuMNs aggregation is readily visible on the slide and was targeted with the focus of the laser. Data was collected on four different spots and the average results are presented.

Capture enrichment-enhancement was performed by adding 50 µl of 1 mg/ml pAb-Lis-AuMNs to 1 ml of various concentrations of *L. monocytogenes* from 10^7–10^4 CFU [Note that these concentrations are within range of 50% predicted morbidity on serious *listeriosis* for high-risk individuals (WHO/FAO, 2004)]. These suspensions were allowed to incubate for 5 min pAb-Lis-AuMNs bound to *L. monocytogenes* were aggregated using an external 35 Gauss permanent Neodymium magnet. Next, the enriched, aggregated sample was pipetted onto the glass substrate. A scheme illustrating this procedure is shown in **Figure 2**.

Probing Interactions Between *L. monocytogenes* and Polyclonal Antibody Gold-coated Magnetic Nanoshells

High-Resolution Scanning Electron Microscopy (HR-SEM) was performed using a Hitachi S-4800 SEM. Imaging was performed on cultures of *L. monocytogenes* after the introduction of Ab-AuMNs to assess binding. A bacterial culture (3 ml) was mixed with 50 µl of pAb-Lis-AuMNs for 5 min. The sample was collected into a pellet *via* magnetic field using a 35 Gauss magnet for 10 min before removing the supernatant. The sample was then fixed using 2 ml of a 2% paraformaldehyde (Alfa Aesar 30525-89-4) in phosphate buffer solution for 24 h at 4°C. Following fixation, cells were washed three times for 10 min in 1X, 7.4 pH PBS. Washed cells were then postfixed using a 2% solution of OsO_4 in phosphate buffer for 24 h at 4°C. After staining, the cells were treated to a series of dehydration in ethanol (30, 40, 50, 60, 70, 80, 90, 95, and 100%) each for 10 min. The sample was then sputtered at 25 mA and 1 kV for 40 s.

Optical microscopy and Gram staining were performed using 100 µl of *L. monocytogenes* diluted to 1E6 CFU ml^{-1} and for necessary samples mixed with 10 µl of Ab-MNPs 5 min. A 10 µl

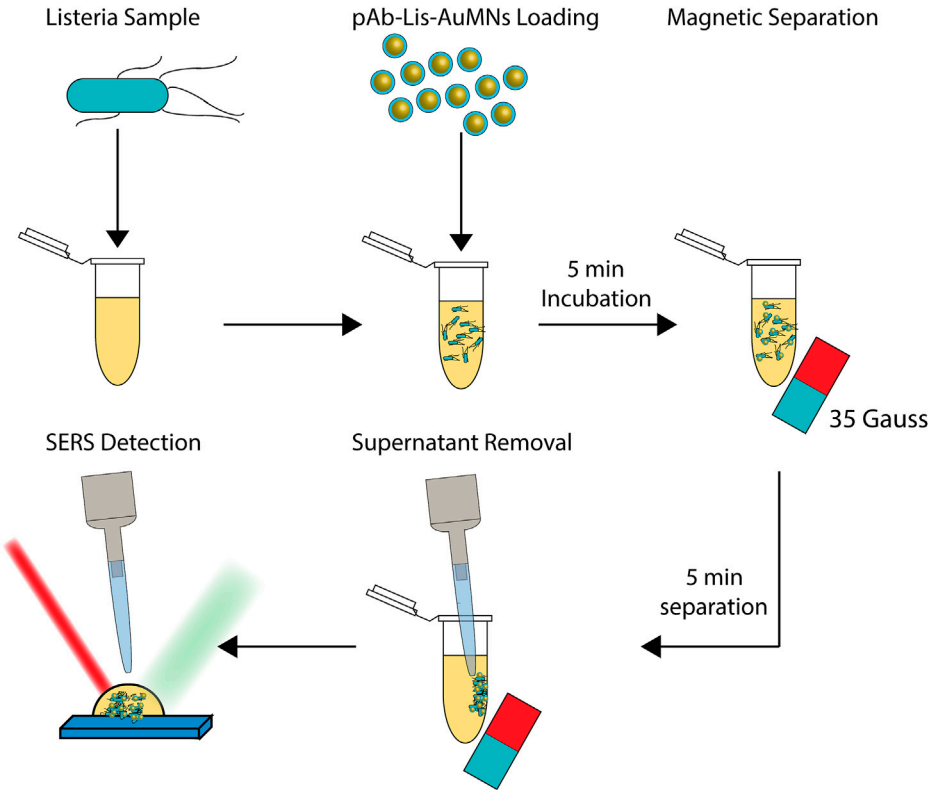

FIGURE 2 | Graphical depiction of SERS enrichment-enhancement method. *Listeria* of a desired concentration is collected. *Listeria monocytogenes* targeting pAb are bound to AuMNs and added to the *L. monocytogenes* sample before incubating for a short time. The *L. monocytogenes* now bound with pAb-Lis-AuMNs are aggregated using a 35 Gauss magnet. Supernatant is then carefully removed before using the enriched sample in the SERS detection. Binding, separation, and detection of *L. monocytogenes* occurs in less than 15 min.

sample was placed on a glass slide and passed through an open flame three times smear side up. The substrate on the glass slide was then flooded with crystal violet for 1 min before gently rinsing with DI water. The substrate was then flooded with Gram's iodine for 1 min before rinsing with DI water. Then, the substrate was decolorized with 95% ethanol added dropwise, until clean, before rinsing with DI water. The sample was air dried until no liquid was visible, and it was viewed directly under oil-immersion using a Quintuple Plan Infinity Kohler Laboratory Trinocular Compound Microscope (1000X). Cell counts were performed utilizing ImageJ with five locations for each sample.

Statistical Methods

The data were analyzed using one-way analysis of variance (ANOVA) for multiple samples or the Students *t*-test to confirm statistical differences. A two-one-sided *t*-test (TOST) was utilized to confirm statistical equivalence. Statistical analysis was performed using JMP Professional v.14. Quantitative data results are expressed as the mean ± standard error of the mean. Statistical differences are represented as * for $p < 0.05$ and ** for $p < 0.01$.

RESULTS AND DISCUSSION

Polyclonal Antibody Gold-coated Magnetic Nanoshells Morphological and Chemical Structure

TEM micrographs showed the general core-shell structural morphology of the AuMNs after pAb-Lis binding (**Figure 3A**). Minor instances of aggregation or interaction and clustering of pAb-Lis-AuMNs of multiple particles were observed, showing the nanoshells' stability after the surface functionalization steps. AuMN diameter by TEM was 278 ± 17 nm (**Supplementary Figure S1**) before pAb-Lis attachment. After surface functionalization of the AuMNs with pAb-Lis, the nanoshell diameter increased to 302 ± 7 nm as observed with TEM. **Figure 3B** shows the developed protein corona layer, a narrow shadow about the AuMNs, measured to be 5.6 ± 1.2 nm thick, comparable to previously reported pAb-Lis thicknesses onto smaller Au nanoparticles of only 40 nm in diameter (Busch et al., 2019). This work confirms the effectiveness of the pAb-Lis binding bioconjugation onto AuMNs of larger sizes (~280 nm). Reported antibody thickness agreed with

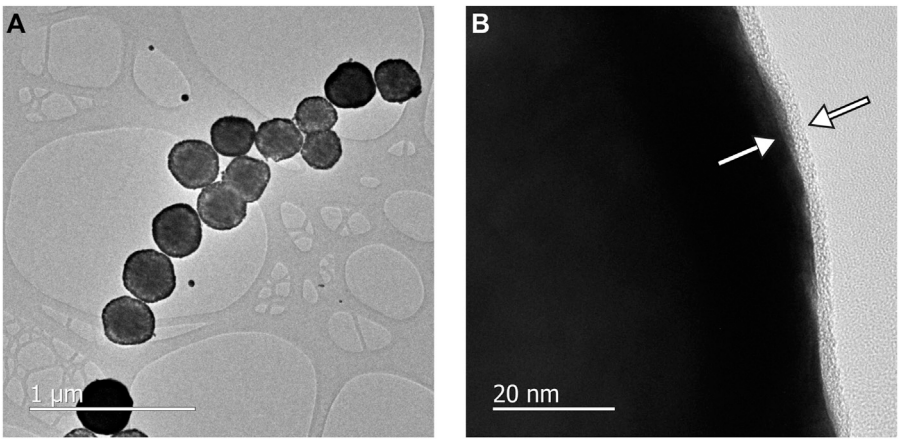

FIGURE 3 | (A) TEM of the pAb-Lis-AuMNs shows the morphology of the particles and aggregation after sample drying, the pAb-Lis-AuMNs exhibited a tendency to form linear chains. **(B)** High resolution TEM of the pAb-Lis-AuMNs shows the consistent corona layer forming around the individual particles, with a pAb thickness of ~5 nm (arrows).

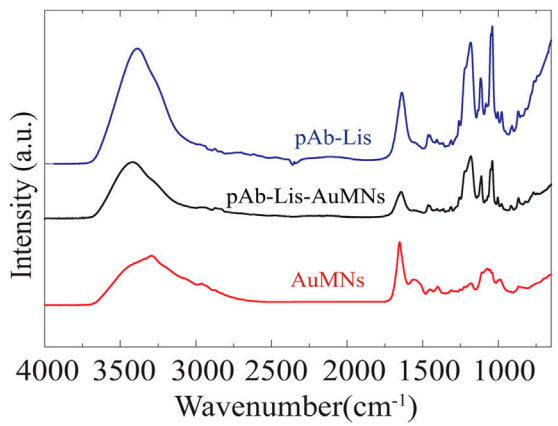

FIGURE 4 | Normalized FT-IR curve showing peak matching between the as-received AuMNs, the pAb-Lis and the pAb-Lis-AuMNs. Note that a full table of peak assignments is shown in **Supplementary Table S1**.

TABLE 1 | Sample identification of 1:2 serial dilutions performed to prepare multiple *L. monocytogenes* solutions at different concentrations.

Sample number	Concentration (CFU/ml)
1st	10^{6}
2nd	$10^{5.7}$
3rd	$10^{5.3}$
4th	$10^{5.1}$
5th	$10^{4.8}$

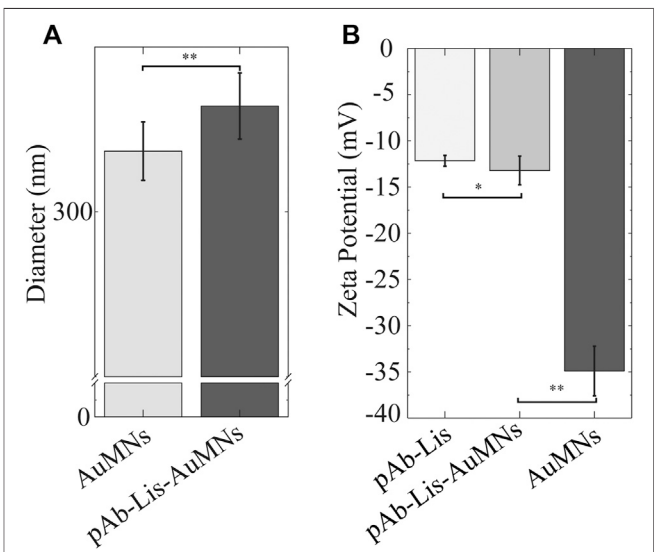

FIGURE 5 | (A) DLS particle size change using effective diameter exhibits a 99% confidence *t*-test suggesting statistically significant change in effective diameter. **(B)** ζ-potential exhibits significance with 95% confidence of equivalence utilizing the TOST test between the pAb-Lis and the pAb-Lis-AuMNs. Simultaneously, the pAb-Lis-AuMNs and the AuMNs exhibit statistical difference with 99% confidence.

additional IgG protein corona thicknesses, ranging from 3.5 to 15 nm depending on the antibody orientation (Ruiz et al., 2019).

Chemical characterization was performed using FT-IR spectroscopy (**Figure 4**; **Supplementary Table S1**). The pAb-Lis, AuMNs, and pAb-Lis-AuMNs spectra were collected to determine chemical structure changes and binding steps. The pAb-Lis-AuMNs spectrum displayed a strong resemblance with the pAb-Lis spectrum, sharing peaks throughout the scanned region. This similitude confirmed that the observed thin layer through TEM corresponded to the pAb-Lis. Notable absorption peaks were identified at 1044, 1117, 1185, and 1455 cm^{-1} in the fingerprint region and amide III regions, as well as a peak at 1638 cm^{-1} and a shoulder at 1554 cm^{-1} in the amide I and II regions, respectively. The AuMNs alone maintained peaks at 1656 and 1543 cm^{-1}, while the fingerprint region held noticeably different peaks from the pAb-Lis-AuMNs at 991, 1076, and

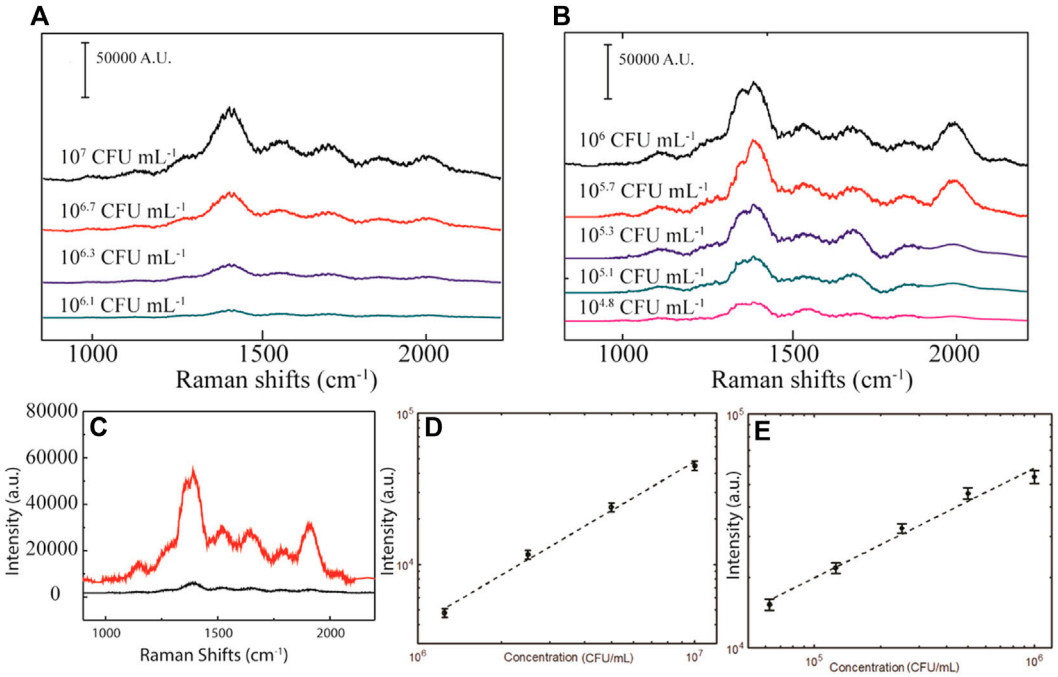

FIGURE 6 | (A) Raman spectrum for *L. monocytogenes* at different concentrations. **(B)** SERS spectrum of the *L. monocytogenes* combined with pAb-Lis-AuMNs. **(C)** Comparison of the Raman spectra at 10^6 CFU ml^{-1} showing dramatic enhancement of the curve after magnetic aggregation. Raman peak intensity at 1388 cm^{-1} for the **(D)** *L. monocytogenes* and **(E)** SERS *L. monocytogenes* with pAb-Lis-AuMNs as a function of the pathogen concentration while under the presence of a magnetic field (35 Gauss).

1182 cm^{-1}. Full peak assignments for each sample are also shown in **Supplementary Table S1**. Direct comparisons of IR peak assignment show representation of nearly all peaks shown for the pAb-Lis and pAb-Lis-AuMNs within a wavenumber of ± 3cm^{-1} (**Table 1**). In fact, several of the AuMNs peaks are no longer present as primary peaks confirming the pAb-Lis coating onto the surface of the AuMNs. Overall, FT-IR results demonstrated the successful bioconjugation of the pAb-Lis onto the AuMNs surface.

DLS measurements were used to analyze the size change and stability of the pAb-Lis-AuMNs as compared to the AuMNs in suspension (**Figure 5A**). The AuMNs maintained an effective diameter of 309.1 ± 4.4 nm, while the pAb-Lis-AuMNs had an effective diameter of 316.1 ± 5.0 nm. This size increase was attributed to a combination of protein bioconjugation and a slight decrease in the AuMNs colloid's stability, causing particles to agglomerate as observed in **Figure 3A**. This decrease in stability was likely due to antibody-bound particles displaying a tendency to agglomerate in aqueous solutions *via* protein-protein interactions(Neupane et al., 2017). This result also explained for the difference between size change observed by DLS as compared with protein corona layer size observed by TEM (**Figure 3B**). To corroborate these results, ζ-potential measurements were conducted, and results are shown in **Figure 5B**. Results confirmed equivalence of charge for the pAb and the pAb-Lis-AuMNs on the nanoshells' surface after bioconjugation. The neat AuMNs held a ζ-potential of -34.9 ± 2.7 mV confirming the presence of -COOH groups on its surface, while the pAb-Lis and pAb-Lis-AuMNs had ζ-potential values of −12.1 ± 0.6 mV and −13.2 ± 1.6 mV, respectively. The different pAb-Lis-AuMNs ζ-potential value, as compared to AuMNs, confirmed the presence of the antibody on the nanoshell surface.

Polyclonal Antibody Gold-coated Magnetic Nanoshells as a SERS Sensing Probe and Bacteria Detection

Control experiments were conducted to confirm that pAb-Lis functionalization plays a vital role in the detection and aggregation of *L. monocytogenes*. The Raman spectrum of neat AuMNs, without antibody modification, in the presence of *L. monocytogenes* is presented (**Supplementary Figure S2**). Additionally, the pAb-Lis-AuMNs Raman spectrum is reported (**Supplementary Figure S3**). A 1:2 serial dilution (**Table 1**) of *L. monocytogenes* from 10^5–10^7 CFU ml^{-1} taken as Raman spectra are shown in **Figures 6A,D** as baseline comparisons. At the 1388 cm^{-1} shift location, the *L. monocytogenes* was found to have a strong correlation with an $R^2 = 0.99$ (**Supplementary Equation S1**). A linear model must be used to determine the limit of detection (LOD) as defined in **Eq. 1**; where SD is the standard deviation of the blank sample, and m is the slope of the linear model. The *L. monocytogenes* without enhancement holds a LOD between 10^4 and 10^5.

Then, the pAb-Lis-AuMNs SERS analysis was performed. Immediately after the addition of the pAb-Lis-AuMNs to a *L.*

monocytogenes solution, a slight increase in signal was observed, followed by a drastic increase upon introduction of a 35 Gauss magnet (**Figure 6C**). The high magnetic moment of the iron-oxide cores of the pAb-Lis-AuMNs provides a scaffold to physically aggregate the *L. monocytogenes,* effectively enhancing the localized concentration. This effect—along with the increased scattering from the plasmon resonance of the gold shell; a well-known surface enhancing measurement of the pAb-Lis-AuMNs—provides the SERS enhancement described below (Halas, 2005; Lal et al., 2008; Ye et al., 2012). A ten-fold diluted series was used for the SERS comparison of the *L. monocytogenes* from 10^4–10^6. The shifts are reported in **Figure 6B** and a correlation (**Figure 6E**) at the 1388 cm^{-1} location shows a strong linear trend, R^2 = 0.96 (**Supplementary Equation S2**) with a limit of detection (LOD) of ~10^3 CFU ml^{-1}. Note that the points shown in **Figure 6E** represent intensity counts from four data sets collected on the visible, aggregated structures observed on the slide after magnetic aggregation, and individual results are shown in **Supplementary Figure S4**. The variation of intensity (ΔI) was calculated using **Eq. 2**, where I_m= minimum or maximum intensity and the average intensity (I_{ave}) as indicated in **Supplementary Figure S4**. Additionally, an enhancement factor (EF) of ~$10^{4.4}$ was found as defined in **Eq. 3**, where I_{SERS} and I_{RS} are the peak intensities of the SERS spectra and the Raman spectra at identical concentrations at the 1388 cm^{-1} locations. N_{Surf} is the average number of adsorbed molecules in the scattering volume for the SERS experiment and N_{Vol} is the average number of molecules in the scattering volume (Kneipp et al., 1998; Le Ru et al., 2007).

$$\mathrm{LOD} = 3\frac{SD}{m} \tag{1}$$

$$\Delta I = \frac{|I_m - I_{ave}|}{I_m} \times 100\% \tag{2}$$

$$\mathrm{EF} = \frac{I_{SERS}/N_{surf}}{I_{RS}/N_{vol}} \tag{3}$$

Using pAb-Lis-AuMNs, a two order of magnitude LOD increase for the direct detection of the *L. monocytogenes* was obtained. Other methods have reported similar sensitivity for SERS-based biosensors, on the order of 10–1000 CFU ml^{-1} (Baniukevic et al., 2013; Zhang et al., 2015; Granger et al., 2016). However, many of these dramatically low SERS methods used a secondary reporter molecule; generally, a gold nanorod optically tuned to the laser intensity to tag the bacteria. This previous work resulted in a SERS curve that maintains the signal probe's characteristics rather than of the pathogen itself. This work presents an important distinction, as the ability to bind to specific strains of pathogens is critical in determining a potential pathogenic outbreak (Liu, 2006). Recently, the use of probes without these secondary labeling, called label-free probes, has garnered interest for this particular reason (Wang et al., 2019), and pAb-Lis-AuMNs demonstrated the potential to detect and aggregate *L. monocytogenes* while in solution. Although there are some high sensitivity *L. monocytogenes* probes and label-free bacteria probes, very few *L. monocytogenes* label-free probes are reported in the literature. For a comparison, examples of previously reported methods and LOD are shown in **Table 2**. To the authors' knowledge, this is the first time a pAb-Lis coated AuMNs have been used for the detection and aggregation of *L. monocytogenes* (Yang et al., 2007; Wang et al., 2010; Wang et al., 2015; Wang et al., 2016b; Tamer et al., 2011; Tolba et al., 2012). The reported method maintains similar sensitivity previously found with alternative SERS based methods on other bacteria such as *E. coli*. Future efforts will focus on understanding the effectiveness of the distinctly labeled pAb-Lis-AuMNs in the detection of *L. monocytogenes* while in the presence of other bacteria, media or matrices, and other cells. Here, we demonstrated for the first time the improved and rapid detection of *L. monocytogenes* while exposed to a low magnetic field, generated by a permanent magnet, under the presence of pAb-Lis-AuMNs.

Aggregation and Magnetic Separation of *L.monocytogenes* Using pAb-Lis-AuMNs

HR-SEM was utilized to show the functional binding of the pAb-Lis-AuMNs onto the cell wall of the *L. monocytogenes*. The aggregation of the *L. monocytogenes* showed tight packing after magnetic aggregation, fixing, post-fixing, and dehydration (**Figure 7A**). Selection of the pAb-Lis-AuMNs as the limiting factor appeared to have caused the magnetic nanoshells to largely remain out of view on the interior of the aggregated *L. monocytogenes* membrane; however, a few exterior particles remained and were observed (**Figures 7A,B**). Due to the size of the pAb-Lis-AuMNs, we visualized the binding of the particles to the *L. monocytogenes* (**Figure 7C**) in an aggregated state, potentially in multiple layers, as previously depicted in **Figure 1**. This analysis confirmed the aggregation and binding of the pAb-Lis-AuMNs to the *L. monocytogenes* walls.

In-situ analysis of the magnetic nanoshells' magnetic effects through SEM was difficult to assess due to the fixing, dehydration, and application of the magnetic field necessary to view the pathogens (De Jonge and Ross, 2011). To overcome this issue, we used a simple Gram staining method to quantify and visualize the enhancement *via* the magnetic aggregation of the *L. monocytogenes* after bioconjugation (Beveridge, 2001). **Supplementary Figures S5–S8** show micrographs collected under optical microscopy of the *L. monocytogenes* at 10^6 CFU ml^{-1} using a 50 Gauss circular magnet. For instance, a pathogen count increase of over 13 times per mm^2 was demonstrated, which is a drastic increase in localized pathogen counts by forming aggregated clusters (**Figure 7D**). This effort provided insights into the advantage of using sub-micron sized magnetic particles as a SERS capture probe for bacteria.

An important distinction of this study as compared to other SERS studies for bacteria detection is the enhancement achieved specifically for *L. monocytogenes*—an understudied bacterium in the SERS field—as well as the use of the polyclonal antibody coatings on the AuMNs (pAb-Lis-AuMNs) surface as the limiting reactant during the binding

TABLE 2 | Previously reported methods for bacteria detection using label-based and label-free probes. *This work is inserted for immediate comparison.

Target	Detection method	Detection limit (CFU/ml)	Label type	References
E. coli	SERS	35	Label-based	Tamer et al. (2011)
E. coli	SERS	10^3	Label-free	Wang et al. (2016a)
S. aureus	SERS	10	Label-based	Wang et al. (2016b)
L. monocytogenes	Fluorescence	50	Label-based	Wang et al. (2010)
L. monocytogenes	Electrochemical	10^4	Label-free	Tolba et al. (2012)
L. monocytogenes	Real-time PCR	10^2	N/A	Yang et al. (2007)
L. monocytogenes	SERS-based lateral flow strip biosensor	17	Label-based	Wang et al. (2010)
L. monocytogenes	SERS	10^3	Label-free	This work*

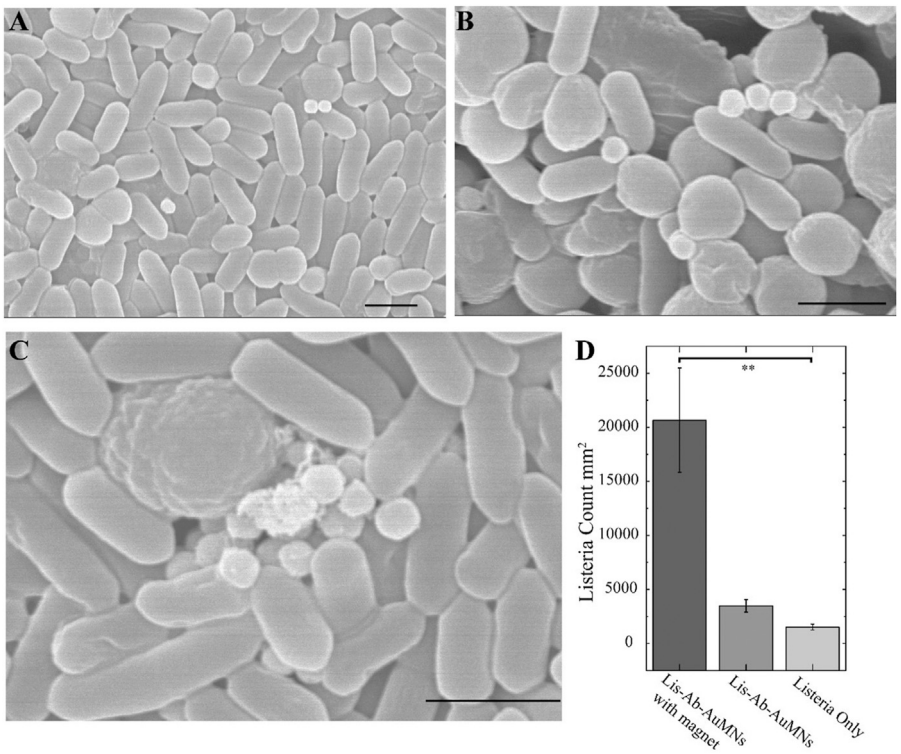

FIGURE 7 | (A) HR-SEM of a general region of the aggregated *L. monocytogenes* displaying a few pAb-Lis-AuMNs on top of the bacteria. **(B, C)** HR-SEM images showing pAb-Lis-AuMNs bound *L. monocytogenes* aggregates while under the presence of a magnet; **(C)** shows multiple pAb-Lis-AuMNs aggregating bacteria in a multilayer structure as depicted in **Figure 1**. **(D)** *L. monocytogenes* counts as determined under optical microscopy utilizing Gram staining exhibits a 99% confidence one-way ANOVA suggesting statistically significant differences in the mean *L. monocytogenes* counts between the three tested conditions. (The scale bar for all images is 1 micron).

protocol. By utilizing the pAb-Lis-AuMNs as the limiting reactant, *L. monocytogenes* bounded by single particles aggregated into clusters with the pAb-Lis-AuMNs generally oriented toward the magnetic source as shown in **Figure 7A**; **Supplementary Figure S5**. This result indicated instances of 1:1 pAb-Lis-AuMNs to *L. monocytogenes* capture held enough interaction to pull the *L. monocytogenes* spatially through a solution. This promising application of submicron pAb-Lis-AuMNs can be extrapolated to more general and industrial uses where binding multiple bacterium or matrices with multiple particles may become burdensome and unrealistic.

CONCLUSION

This study confirmed the fabrication and characterization of polyclonal *Listeria* antibody functionalized gold-coated iron oxide nanoshells (pAb-Lis-AuMNs), with approximately 300 nm in size. These sub-micron probes have the potential to adhere to *L. monocytogenes* and serve as SERS probes, which can be used for biosensing and bacteria separation. As a SERS probe, pAb-Lis-AuMNs demonstrated a limit of detection of ~10^3 CFU ml^{-1}. Overall, the proposed label-free methodology using magnetic nanoshells shows high sensitivity and a 5 min rapid detection time for *L. monocytogenes*. Additional capture and

separation of bacteria under a low magnetic field using a permanent magnet in only 5 min were possible using the as-prepared, sub-micron sized functionalized magnetic nanoshells. With the proper antibody, results from this work could be extended to other types of bacteria and selective separation and sorting from different matrices and applied external magnetic fields.

DATA AVAILABILITY STATEMENT

The raw data supporting the conclusions of this article will be made available by the authors, without undue reservation.

AUTHOR CONTRIBUTIONS

RB: Investigation, Visualization, Formal Analysis, Writing-Original Draft, Conceptualization and Data Curation; FK: Investigation, Formal Analysis, Review and Editing; YS: Investigation, Formal Analysis, Review and Editing, Project administration, Funding; CF: Investigation, Review and Editing; YL: Investigation, Review and Editing; CZ: Investigation, Formal Analysis, Review and Editing, Project administration, Funding; EV: Conceptualization, Formal analysis, Resources, Data Curation, Visualization, Writing—Review and Editing, Supervision, Project administration, Funding.

FUNDING

Funding available through the University of Dayton STEM Catalyst Initiative, Integrative Science and Engineering Center, and the Graduate Student Summer Fellowship. Funding for Open Access provided by the University of Dayton Open Access Fund and the Integrative Science and Engineering Center. Use of the Center for Nanoscale Materials, an Office of Science user facility, was supported by the United States Department of Energy, Office of Science, Office of Basic Energy Sciences, under Contract No. DE-AC02-06CH11357.

SUPPLEMENTARY MATERIAL

The Supplementary Material for this article can be found online at: https://www.frontiersin.org/articles/10.3389/fnano.2021.653744/full#supplementary-material

REFERENCES

Baniukevic, J., Hakki Boyaci, I., Goktug Bozkurt, A., Tamer, U., Ramanavicius, A., and Ramanaviciene, A. (2013). Magnetic Gold Nanoparticles in SERS-Based Sandwich Immunoassay for Antigen Detection by Well Oriented Antibodies. *Biosens. Bioelectron.* 43, 281–288. doi:10.1016/j.bios.2012.12.014

Bao, F., Yao, J.-L., and Gu, R.-A. (2009). Synthesis of Magnetic Fe2O3/Au Core/shell Nanoparticles for Bioseparation and Immunoassay Based on Surface-Enhanced Raman Spectroscopy. *Langmuir* 25, 10782–10787. doi:10.1021/la901337r

Bartczak, D., and Kanaras, A. G. (2011). Preparation of Peptide-Functionalized Gold Nanoparticles Using One Pot EDC/Sulfo-NHS Coupling. *Langmuir* 27, 10119–10123. doi:10.1021/la2022177

Beveridge, T. J. (2001). Use of the Gram Stain in Microbiology. *Biotech. Histochem.* 76 (3), 111–118. doi:10.1080/bih.76.3.111.118

Buchanan, R. L., Gorris, L. G. M., Hayman, M. M., Jackson, T. C., and Whiting, R. C. (2017). A Review of Listeria Monocytogenes : An Update on Outbreaks, Virulence, Dose-Response, Ecology, and Risk Assessments. *Food Control* 75, 1–13. doi:10.1016/j.foodcont.2016.12.016

Busch, R. T., Karim, F., Weis, J., Sun, Y., Zhao, C., and Vasquez, E. S. (2019). Optimization and Structural Stability of Gold Nanoparticle-Antibody Bioconjugates. *ACS Omega* 4, 15269–15279. doi:10.1021/acsomega.9b02276

Chen, H., Das, A., Bi, L., Choi, N., Moon, J.-I. L., Wu, Y., et al. (2020). Recent Advances in Surface-Enhanced Raman Scattering-Based Microdevices for Point-Of-Care Diagnosis of Viruses and Bacteria. *Nanoscale* 12, 21560–21570. doi:10.1039/d0nr06340a

De Jonge, N., and Ross, F. M. (2011). Electron microscopy of specimens in liquid. *Nat. Nanotechnol.* 6 (11), 695–704. doi:10.1038/nnano.2011.161

Dörig, P., Stiefel, P., Behr, P., Sarajlic, E., Bijl, D., Gabi, M., et al. (2010). Force-controlled Spatial Manipulation of Viable Mammalian Cells and Micro-organisms by Means of FluidFM Technology. *Appl. Phys. Lett.* 97, 023701. doi:10.1063/1.3462979

Food, E., and Authority, S. (2013). Analysis of the Baseline Survey on the Prevalence of *Listeria Monocytogenes* in Certain Ready-To-Eat Foods in the EU, 2010-2011 Part A: *Listeria Monocytogenes* Prevalence Estimates. *EFSA J.* 11, 3241. doi:10.2903/j.efsa.2013.3241

Fratila, R. M., Mitchell, S. G., Del Pino, P., Grazu, V., and De La Fuente, J. M. (2014). Strategies for the Biofunctionalization of Gold and Iron Oxide Nanoparticles. *Langmuir* 30, 15057–15071. doi:10.1021/la5015658

Granger, J. H., Schlotter, N. E., Crawford, A. C., and Porter, M. D. (2016). Prospects for Point-of-Care Pathogen Diagnostics Using Surface-Enhanced Raman Scattering (SERS). *Chem. Soc. Rev.* 45, 3865–3882. doi:10.1039/c5cs00828j

Grubisha, D. S., Lipert, R. J., Park, H.-Y., Driskell, J., and Porter, M. D. (2003). Femtomolar Detection of Prostate-specific Antigen: An Immunoassay Based on Surface-Enhanced Raman Scattering and Immunogold Labels. *Anal. Chem.* 75, 5936–5943. doi:10.1021/ac034356f

Halas, N. (2005). Playing with Plasmons: Tuning the Optical Resonant Properties of Metallic Nanoshells. *MRS Bull.* 30, 362–367. doi:10.1557/mrs2005.99

Hoffmann, S., Batz, M. B., and Morris, J. G. (2012). Annual Cost of Illness and Quality-Adjusted Life Year Losses in the United States Due to 14 Foodborne Pathogens. *J. Food Prot.* 75, 1292–1302. doi:10.4315/0362-028X.JFP-11-417

Jarvis, R. M., and Goodacre, R. (2008). Characterisation and Identification of Bacteria Using SERS. *Chem. Soc. Rev.* 37, 931–936. doi:10.1039/b705973f

Karim, F., Vasquez, E. S., Sun, Y., and Zhao, C. (2019). Optothermal Microbubble Assisted Manufacturing of Nanogap-Rich Structures for Active Chemical Sensing. *Nanoscale* 11, 20589–20597. doi:10.1039/C9NR05892C

Kneipp, K., Kneipp, H., Manoharan, R., Hanlon, E. B., Itzkan, I., Dasari, R. R., et al. (1998). Extremely Large Enhancement Factors in Surface-Enhanced Raman Scattering for Molecules on Colloidal Gold Clusters. *Appl. Spectrosc.* 52, 1493–1497. doi:10.1366/0003702981943059

Lal, S., Grady, N. K., Kundu, J., Levin, C. S., Lassiter, J. B., and Halas, N. J. (2008). Tailoring Plasmonic Substrates for Surface Enhanced Spectroscopies. *Chem. Soc. Rev.* 37, 898–911. doi:10.1039/b705969h

Law, J. W. F., Ab Mutalib, N. S., Chan, K. G., and Lee, L. H. (2015). Rapid methods for the detection of foodborne bacterial pathogens: principles, applications, advantages and limitations. *Front. Microbiol.* 5, 770.

Le Ru, E. C., Blackie, E., Meyer, M., and Etchegoin, P. G. (2007). Surface Enhanced Raman Scattering Enhancement Factors: A Comprehensive Study. *J. Phys. Chem. C.* 111, 13794–13803. doi:10.1021/jp0687908

Lipman, N. S., Jackson, L. R., Trudel, L. J., and Weis-Garcia, F. (2005). Monoclonal versus Polyclonal Antibodies: Distinguishing Characteristics, Applications, and Information Resources. *ILAR J.* 46, 258–268. doi:10.1093/ilar.46.3.258

Liu, D. (2006). Identification, Subtyping and Virulence Determination of Listeria Monocytogenes, an Important Foodborne Pathogen. *J. Med. Microbiol.* 55, 645–659. doi:10.1099/jmm.0.46495-0

Liu, Y., Zhou, H., Hu, Z., Yu, G., Yang, D., and Zhao, J. (2017). Label and Label-free Based Surface-Enhanced Raman Scattering for Pathogen Bacteria Detection: A Review. *Biosens. Bioelectron.* 94, 131–140. doi:10.1016/j.bios.2017.02.032

Mandal, P. K., Biswas, A. K., Choi, K., and Pal, U. K. (2011). Methods for Rapid Detection of Foodborne Pathogens: An Overview. *Am. J. Food Technology* 6, 87–102. doi:10.3923/ajft.2011.87.102

Montenegro, J.-M., Grazu, V., Sukhanova, A., Agarwal, S., de la Fuente, J. M., Nabiev, I., et al. (2013). Controlled Antibody/(bio-) Conjugation of Inorganic Nanoparticles for Targeted Delivery. *Adv. Drug Deliv. Rev.* 65, 677–688. doi:10.1016/j.addr.2012.12.003

Neupane, S., Pan, Y., Takalkar, S., Bentz, K., Farmakes, J., Xu, Y., et al. (2017). Probing the Aggregation Mechanism of Gold Nanoparticles Triggered by a Globular Protein. *J. Phys. Chem. C.* 121, 1377–1386. doi:10.1021/acs.jpcc.6b11963

Nikoobakht, B., and El-Sayed, M. A. (2003). Surface-Enhanced Raman Scattering Studies on Aggregated Gold Nanorods. *J. Phys. Chem. A.* 107, 3372–3378. doi:10.1021/jp026770+

Ruiz, G., Tripathi, K., Okyem, S., and Driskell, J. D. (2019). PH Impacts the Orientation of Antibody Adsorbed onto Gold Nanoparticles. *Bioconjug. Chem.* 30, 1182–1191. doi:10.1021/acs.bioconjchem.9b00123

Sharma, V., Sinha, N., Dutt, S., Chawla, M., and Siril, P. F. (2016). Tuning the Surface Enhanced Raman Scattering and Catalytic Activities of Gold Nanorods by Controlled Coating of Platinum. *J. Colloid Interf. Sci.* 463, 180–187. doi:10.1016/j.jcis.2015.10.036

Shibusawa, K., Hase, T., and Tsukada, K. (2019). Increasing Surface-Enhanced Raman Scattering Density Using Gold-Coated Magnetic Nanoparticles Controlled *via* a Magnetic Field for Sensitive and Efficient Biomarker Detection. *AIP Adv.* 9, 065316. doi:10.1063/1.5102083

Sposito, A. J., Kurdekar, A., Zhao, J., and Hewlett, I. (2018). Application of Nanotechnology in Biosensors for Enhancing Pathogen Detection. *WIREs Nanomed Nanobiotechnol* 10, e1512–e1522. doi:10.1002/wnan.1512

Tamer, U., Boyacı, İ. H., Temur, E., Zengin, A., Dincer, İ., and Elerman, Y. (2011). Fabrication of Magnetic Gold Nanorod Particles for Immunomagnetic Separation and SERS Application. *J. Nanopart Res.* 13, 3167–3176. doi:10.1007/s11051-010-0213-y

Thakur, M., Asrani, R. K., and Patial, V. (2018). Listeria Monocytogenes: A Food-Borne Pathogen. *Foodborne Dis.* 55, 157–192. doi:10.1016/B978-0-12-811444-5.00006-3

Tolba, M., Ahmed, M. U., Tlili, C., Eichenseher, F., Loessner, M. J., and Zourob, M. (2012). A Bacteriophage Endolysin-Based Electrochemical Impedance Biosensor for the Rapid Detection of Listeria Cells. *Analyst* 137, 5749–5756. doi:10.1039/c2an35988j

U.S. FDA (2020). Get the Facts about Listeria. Available at: https://www.fda.gov/animal-veterinary/animal-health-literacy/get-facts-about-listeria (Accessed March 30, 2021).

Wang, C., Meloni, M. M., Wu, X., Zhuo, M., He, T., Wang, J., et al. (2019). Magnetic Plasmonic Particles for SERS-Based Bacteria Sensing: A Review. *AIP Adv.* 9, 010701. doi:10.1063/1.5050858

Wang, C., Rong, Z., Wang, J., Jiang, N., Pang, Y., Xiao, R., et al. (2016a). Seed-mediated Synthesis of High-Performance Silver-Coated Magnetic Nanoparticles and Their Use as Effective SERS Substrates. *Colloids Surf. A: Physicochemical Eng. Aspects* 506, 393–401. doi:10.1016/J.COLSURFA.2016.05.103

Wang, C., Wang, J., Li, M., Qu, X., Zhang, K., Rong, Z., et al. (2016b). A Rapid SERS Method for Label-free Bacteria Detection Using Polyethylenimine-Modified Au-Coated Magnetic Microspheres and Au@Ag Nanoparticles. *Analyst* 141, 6226–6238. doi:10.1039/c6an01105e

Wang, J., Wu, X., Wang, C., Shao, N., Dong, P., Xiao, R., et al. (2015). Magnetically Assisted Surface-Enhanced Raman Spectroscopy for the Detection ofStaphylococcus aureusBased on Aptamer Recognition. *ACS Appl. Mater. Inter.* 7, 20919–20929. doi:10.1021/acsami.5b06446

Wang, L., Park, H.-Y., Lim, S. I.-I., Schadt, M. J., Mott, D., Luo, J., et al. (2008). Core@shell Nanomaterials: Gold-Coated Magnetic Oxide Nanoparticles. *J. Mater. Chem.* 18, 2629–2635. doi:10.1039/b719096d

Wang, Z., Miu, T., Xu, H., Duan, N., Ding, X., and Li, S. (2010). Sensitive Immunoassay of Listeria Monocytogenes with Highly Fluorescent Bioconjugated Silica Nanoparticles Probe. *J. Microbiol. Methods* 83, 179–184. doi:10.1016/j.mimet.2010.08.013

Welch, N. G., Scoble, J. A., Muir, B. W., and Pigram, P. J. (2017). Orientation and Characterization of Immobilized Antibodies for Improved Immunoassays (Review). *Biointerphases* 12, 02D301. doi:10.1116/1.4978435

World Health Organization/Food and Agriculture Organization of the United Nations (WHO/FAO) (2004). Risk Assesment of *Listeria Monocytogenes* in Ready-To-Eat Foods. Available at: http://www.fao.org/fileadmin/templates/agns/pdf/jemra/mra4_en.pdf (Accessed March 30, 2021).

Wu, X., Huang, Y.-W., Park, B., Tripp, R. A., and Zhao, Y. (2015). Differentiation and Classification of Bacteria Using Vancomycin Functionalized Silver Nanorods Array Based Surface-Enhanced Raman Spectroscopy and Chemometric Analysis. *Talanta* 139, 96–103. doi:10.1016/j.talanta.2015.02.045

Yang, H., Qu, L., Wimbrow, A. N., Jiang, X., and Sun, Y. (2007). Rapid Detection of Listeria Monocytogenes by Nanoparticle-Based Immunomagnetic Separation and Real-Time PCR. *Int. J. Food Microbiol.* 118, 132–138. doi:10.1016/j.ijfoodmicro.2007.06.019

Ye, J., Wen, F., Sobhani, H., Lassiter, J. B., Van Dorpe, P., Nordlander, P., et al. (2012). Plasmonic Nanoclusters: Near Field Properties of the Fano Resonance Interrogated with SERS. *Nano Lett.* 12, 1660–1667. doi:10.1021/nl3000453

Yueming, Z., Junfeng, Z., Yuling, W., Shaojun, G., Wen, R., and Shaojun, D. (2009). Fabrication of Iron Oxide Core/Gold Shell Submicrometer Spheres with Nanoscale Surface Roughness for Efficient Surface-Enhanced Raman Scattering. *J. Phys. Chem. C.* 113, 7009–7014. doi:10.1021/jp810561q

Zhang, H., Ma, X., Liu, Y., Duan, N., Wu, S., Wang, Z., et al. (2015). Gold Nanoparticles Enhanced SERS Aptasensor for the Simultaneous Detection of *Salmonella typhimurium* and *Staphylococcus aureus*. *Biosens. Bioelectron.* 74, 872–877. doi:10.1016/j.bios.2015.07.033

Zhang, Q., Li, R.-X., Chen, X., He, X.-X., Han, A.-L., Fang, G.-Z., et al. (2017). Study of Efficiency of Coupling Peptides with Gold Nanoparticles. *Chin. J. Anal. Chem.* 45, 662–667. doi:10.1016/S1872-2040(17)61013-2

Conflict of Interest: The authors declare that the research was conducted in the absence of any commercial or financial relationships that could be construed as a potential conflict of interest.